IV.4. Iron Fischer-Tropsch Catalysts: Preparation by Oxidation of Aqueous Suspension of $Fe(OH)_2$. (Sivaraj Chokkaram, Ram Srinivasan, Diane R. Milburn, and Burtron H. Davis)

IV.4.1. ABSTRACT

Aqueous ferrous hydroxide suspensions, precipitated from different initial mole ratios of Fe^{2+}:OH^- (R) ranging from 0.2 to 3.0 were oxidized with oxygen or aqueous hydrogen peroxide solution. Similar oxidation experiments were performed at a fixed value of Fe^{2+}:OH^- = 3.0 by varying the oxidation temperature ranging from 7 to 75°C. The product iron oxides/oxyhydroxides were characterized using BET, XRD, and TEM techniques. The results indicated that the R factor as well as the oxidation temperature has a definite effect on the morphology, crystal size and crystal structure of the product iron oxyhydroxide or oxide.

IV.4.2. INTRODUCTION

Iron oxides, oxyhydroxides and hydroxides play an important role in a variety of applications, such as catalysts, co-catalysts, pigments, magnetic materials., etc. For most of these applications very specific type of starting iron compounds are necessary. Since the method of preparation is a key factor in controlling the physico-chemical properties, especially their structure and texture, it is essential to establish suitable experimental conditions to produce the desired iron oxyhydroxide or oxide. In general, iron oxyhydroxides or oxides may be prepared by oxidation of aqueous suspensions ferrous hydroxide or by precipitating from a solutions of a ferric salt with a suitable precipitating agent, followed by dehydration and or dehydroxylation process. In all these processes the pH, of precipitation the initial ionic strength of the

solution, the concentration of the iron solution, the anions that are present and other experimental conditions may play a role in determining the final structure of the iron oxyhydroxide or oxide.

Although the oxidation process of aqueous $Fe(OH)_2$ suspension and the mechanism of formation of iron oxyhydroxides and oxides have been studied by several researchers for example (IV.4.1-IV.4.11), there are very few reports which relate the physico-chemical properties of the resulting oxyhydroxides or oxides with respect to their preparation methods. Olowe and Genin (IV.4.1) studied the oxidation process of aqueous ferrous hydroxide suspensions and considered the mechanism of Fe^{2+} oxidation, including the effect of initial Fe^{2+}:OH^- ratio (R) on the product. The formation of FeOOH species from Fe(II) hydroxide was shown by Bernal et al (IV.4.2) to proceed through an intermediate Green Rust species. It has been demonstrated by several authors (IV.4.3-IV.4.11) that the anions present in the suspension (e.g., Cl^-, SO_4^{2-}, CO_3^{2-} etc.,) can strongly influence the structure and composition of the intermediate Green Rust complex. Hansen (IV.4.7) reported the formation of a pyroaurite-type compound of Fe(II) Fe(III) hydroxy-carbonate (GR) by the induced hydrolysis of ferrhydrite and Fe(II) chloride at a pH= 7.00. This author also reported that a stoichiometric compound, $Fe_2^{III}Fe_4^{II}(OH)_2\ CO_3$, was formed, and that the Fe(II):Fe(III) ratio was not dependent on the overall Fe(II):Fe(III) ratio in the reaction mixture. Feitknecht (IV.4.8) and Allman (IV.4.9) suggested that the Green Rust is a particular case of mixed hydroxides possessing the pyroaurite-sjogrenite structure. This structure consists of planar layers of octahedra in which the metal atom occupies the center and the OH^- groups occupy the corners. The structure of this layer is

identical with that of layers in the crystal lattice of hydroxides of some of divalent metals such as $Fe(OH)_2$ or $Ni(OH)_2$. Recently Clarke and Hall (IV.4.11) reported the preparation and interconversion of iron oxyhydroxides or oxides. They used X-ray diffraction and small angle neutron scattering (SANS) techniques for the characterization of iron oxyhydroxides or oxides. Their SANS study on α-Fe_2O_3, γ-Fe_2O_3 and Fe_3O_4 show nonlinear Gunier behavior; on the other hand, the Debye analysis showed linear plots indicating a random structure. In the present study we evaluated the effect of the $[Fe^{2+}]/[OH^-]$ ratio (R), the oxidizing agent, the rate of oxidation, and the oxidation temperature on the crystal structure, morphology, BET surface area, pore structure and crystal size of the iron oxyhydroxides or oxides.

IV.4.3. EXPERIMENTAL

IV.4.3.a. (i) Preparation

Ferrous hydroxide was precipitated from an aqueous solution of ferrous sulfate (0.2 M) by the addition of aqueous sodium hydroxide solution (5.0 M). The resulting grey suspension of ferrous hydroxide was then oxidized with molecular oxygen or aqueous H_2O_2. After completion of the oxidation process the products were collected by filtration, washed and then dried in air at 90°C for 24 hrs. Experiments were conducted at a number of initial pH values of the ferrous hydroxide suspension (i.e by varying R, [Fe]/[OH] mole ratio) and also at different temperatures ranging from 7 to 75°C at a constant mole ratio of $[Fe]/[OH^-]$ equal to 3.00.

In a typical experiment, 83.4 grams of $FeSO_4 \cdot 7H_2O$ was dissolved in 1500 ml of distilled and deionized water, through which had been flushed for 30 minutes with a nitrogen gas flow to remove dissolved oxygen. Then aqueous sodium hydroxide (5M)

was added drop-wise with constant stirring to produce the required pH value. The resulting grey suspension was oxidized by bubbling dry oxygen (45 cc/min.) through the suspension. The pH of the mixture was monitored with a Orion pH meter (Model number 420). After completion of the oxidation, the precipitate was filtered, washed and dried.

Oxidation with aqueous H_2O_2 was effected by adding excess amount of H_2O_2 greater than required for the oxidation of total the iron(II). The reaction mixture was stirred vigorously during the addition of aqueous H_2O_2. The resulting precipitate was filtered, washed and dried.

IV.4.3.b. (ii) BET Surface Areas and Pore Size Distribution

A Quantachrome Autosorb 6 instrument was used for nitrogen sorption isotherms measurements. The sample was outgassed at 80°C and < 5 mtorr for at least 8 hrs. The surface area was calculated using the BET equation (IV.4.12) and the nitrogen sorption data. Pore size distributions were calculated from the desorption data assuming a cylindrical pore shape with refinements developed by Broekhoff and deBoer (IV.4.13) which correct for the adsorbed layer of nitrogen. This model was chosen over packed particle models or cylindrical pore models because it provides better agreement with the BET surface area and Gurvitsch pore volume.

IV.4.3.c. (iii) X-Ray Diffraction Measurements

X-Ray diffraction studies were carried using a Philips X-ray diffractometer operating at 25kv, 20 mA, and CuKα radiation (λ=1.5418 A). The identification of the phases present in the product was accomplished by overlaying the standard ASTM diffraction pattern of an expected compound. The exactly matched diffraction peaks

were marked accordingly. This process was repeated with several expected iron compounds which enabled an identification of the various phases in the sample.

IV.4.3.d. (iv) TEM and Electron Microdiffraction

To prepare a specimen for examination by TEM, a few milligrams of the powdered sample was suspended in absolute ethanol. This suspension was agitated in an ultrasonic bath and then a drop of the suspension was placed on a carbon coated copper grid. The alcohol evaporated leaving a film of catalyst particles on the grid, which was then loaded into a Hitachi H800 NA scanning transmission electron microscope (STEM). The operating voltage was 200 kV. Microdiffraction and energy-dispersive X-ray (EDX) analysis were carried out in the nanoprobe mode (2 or 5 nm in diameter). This microscope is equipped with a silicon-lithium diode detector (Link) and a multi-channel analyzer (Tracer 500). The X-rays emitted from the specimen upon electron irradiation were collected in the range 0-20 keV for 60 s.

IV.4.4. RESULTS

IV.4.4.a. Precipitation

Precipitation and oxidation experiments were carried out in batch experiments. During oxidation, the grey color first changed to dark-green indicating the formation of Green Rust (IV.4.14). The color then changed to yellow, orange yellow or dark depending on the initial [Fe]/[OH] mole ratio, the oxidizing agent and the oxidation temperature. In the present investigation yellow precipitates were observed when the initial mole ratio of [Fe]/[OH] was >3.00 or <0.2 and gaseous oxygen was used as the oxidizing agent. The formation of a dark brown/black precipitate was observed when the initial mole ratio of [Fe]/[OH] was 0.50. When the initial [Fe]/[OH] mole ratio

was <0.50 and the oxidizing agent was aqueous hydrogen peroxide the color of the precipitate was yellow-orange.

The change in pH with time is shown in Figure IV.4.1 for oxidation at different temperatures. The pH changes are different at each oxidation temperature, and the rate increases with an increase in temperature. Two steps are observed for each curve in Figure IV.4.1. From the pH and the oxidation time data, the derivative d(pH)/dt vs oxidation time plots were generated to obtain the time for each of the two inflection points t_1 and t_2. It was observed that the conversion of the oxygen, i.e. the flow out - flow in, increased with increasing reaction temperature. The solubility of oxygen in water decreases with increasing temperature. Plots of the $\ln(t_1)$ and $\ln(t_2)$ vs 1/T for each step of the pH vs time curves (Figure IV.4.2) exhibit an Arrhenius type plot. The activation energy for each step is about 3.6 to 3.7 kcal/mole. These activation energy values are those expected for a diffusion process (E_s). The results suggests that the oxidation of Fe^{2+} in slightly alkaline solution is diffusion controlled.

BET surface areas and XRD results are summarized in Tables IV.4.1 and IV.4.2. The surface areas of the samples precipitated at different [Fe]/[OH] mole ratios at room temperature range from 16 to 60 m^2/g. The surface areas of the samples prepared at different temperatures but at constant [Fe]/[OH] mole ratio of 3.00 vary from 40 to 89 m^2/g, and gradually decrease with increasing oxidation temperature (Figure IV.4.3). The surface areas of α-FeOOH samples prepared from Fe^{2+} salt solutions are in general low compared to those prepared from a Fe^{3+} salt solution.

Nitrogen adsorption-desorption isotherms for samples oxidized with O_2 at various temperatures (Figure IV.4.4) show that those samples oxidized at the lower temperatures (7, 20 and 40°C) have type II adsorption-desorption isotherms. These are typical of nonporous or macroporous material (IV.4.15). The samples prepared at higher temperatures (55 and 75°C) have type IV isotherms with hysteresis which is commonly associated with capillary condensation in mesopores. The pore size distribution, shown in Figure IV.4.5, reflects this trend. Wide distributions of large pores (radius >100 A) are observed for samples oxidized at temperatures lower than 55°C while samples oxidized at 55 and 75°C show a narrower distribution with a maximum at approximately 70 and 90°A, respectively.

X-Ray diffraction results (Tables IV.4.1 and IV.4.2) show that the crystalline form of the final oxidation product depends on the initial mole ratio of [Fe]/[OH], the oxidizing agent and the temperature. For example, at [Fe]/[OH] mole ratios of 3.00 or 0.20 the final product is α-FeOOH when gaseous oxygen is used for the oxidation. Under these same conditions, when the [Fe]/[OH] mole ratio is 0.5 the product is Fe_3O_4. The XRD patterns of these samples are summarized in Figure IV.4.6. To provide understanding of the effect of the oxidizing agent on the nature and crystallinity of the final product, the above experiments were carried out using aqueous hydrogen peroxide as the oxidizing agent (Table IV.4.1 and Figure IV.4.6). These results show that the products are different from those obtained for oxygen. For oxidation with aqueous hydrogen peroxide at a mole ratio of [Fe]/[OH] =3.00, the product is essentially amorphous while at a ratio of 0.20 the product is δ-FeOOH, with small amounts of α-FeOOH.

The XRD results of the samples prepared at different oxidation temperatures and at a constant mole ratio of 3.00 indicate the presence of α-FeOOH phase at all the temperatures studied but at 75°C the product also contains α-Fe_2O_3 in addition to α-FeOOH phase (Table IV.4.2 and Figure IV.4.7). Even though all the samples show the α-FeOOH phase, the crystallinity varied systematically with the oxidation temperature, increasing with oxidation temperature. The crystallite sizes for these samples were calculated from the line broadening technique (IV.4.16). The effect of oxidation temperature on the crystallite sizes at various hkl values is to increase the crystallite sizes gradually in all planes (Figure IV.4.8).

The TEM pictures of an α-FeOOH sample, prepared at a [Fe]/[OH] mole ratio of 3.00, 55°C oxidation temperature and gaseous oxygen show rod shape particles with an average particle length of 150 to 200nm (Figures IV.4.9 and IV.4.10). The Fe_3O_4 sample prepared from ferrous hydroxide aqueous suspension by oxidation with oxygen at room temperature and [Fe]/[OH] mole ratio of 0.50 contains particles that are mostly rectangular or hexagonal in shape, with few rod shape particles (Figure IV.4.11). The average particle diameter is about 50-80nm (Figure IV.4.12) with a wide distribution of sizes. The XRD data of this sample indicate that Fe_3O_4, and no other phase is present. Figure IV.4.13 show the morphology and Figure IV.4.14, the particle size distribution of the δ-FeOOH prepared at [Fe]/[OH] mole ratio of 0.20 using aqueous hydrogen peroxide as the oxidizing agent. This sample differs from those of the α-FeOOH and Fe_3O_4 samples and exhibits mostly hexagonal particles with few rod like shape particles. The length of the few rod like particles is much less than those of α-FeOOH particles.

An electron micrograph obtained from the sample precipitated at 7°C (Figure IV.4.15) shows regions representing large agglomerates without a well-defined particle morphology. A few regions of needle-shape particle morphology can be seen; however, the number of these needles is minimal when compared to the presence of large agglomerates with no well-defined morphology. This result is in agreement with the X-ray diffraction data for this sample which indicates that this sample has poor crystallinity. Several electron micrographs were obtained from the sample precipitated at 40°C. A typical electron micrograph from this sample (Figure IV.4.16) shows long-needle type particles. An electron microdiffraction pattern obtained from one of the needles is shown in the inset of Figure IV.4.16 and indicates the particle is α-FeOOH. The entire sample exhibits this kind of morphology. The microdiffraction results agree with the XRD data.

The sample prepared at 75°C exhibits both long needle-type as well as spherical-type morphologies (Figure IV.4.17). Electron microdiffraction data revealed that the needle-type particles are α-FeOOH and the spherical particles are α-Fe_2O_3 (Figure IV.4.18 (a) and (b) respectively). The electron microdiffraction patterns from the needle-type particles consistently showed α-FeOOH orthorhombic structure and those from the spherical particles exhibited α-Fe_2O_3 rhombohedral structure. The XRD data for

this sample agree with the electron microscopy data.

The length/width (L/W) ratios for the iron oxyhydroxide particles prepared at various temperatures ranging from 20 to 75°C are shown in Figures IV.4.19-IV.4.21. The maximum L/W values vary from 3 to 27 at the oxidation temperatures studied.

However, the L/W values change systematically with the oxidation temperature. For example, the sample prepared at 20°C has L/W values that range from 6 to 27 with most of the particles being in the range of 6 to 18. At 40°C the L/W values vary between 3 and 21. A comparison of the L/W values for the particles prepared at 20 and 40°C shows that the L/W ratios shift slightly toward lower values for the sample prepared at 40°C compared to 20°C. A further increase in the oxidation temperature did not effect the overall L/W distribution (i.e 3 to 27). However, maximum population L/W values vary systematically; for oxidation temperatures of 20, 40, 55 and 75°C the L/W values are in the range of 5-12, 9-12, 6-9, and 3-6 respectively. The results demonstrate that the particle width increases with an increase in oxidation temperature. Apart from this, it is also observed that as the oxidation temperature increases the particle size (length) increases to a maximum value, with further increase in the oxidation temperature the needle-type particles broke/or modify into a cluster of α-Fe_2O_3 spherical particles (see Figures IV.4.17 and IV.4.18). Thus, the formation of thin, elongated needle shape particles occurs during the oxidation of aqueous ferrous hydroxide in a particular temperature range of 20 to 75° C. At low oxidation temperatures the particles are not well defined and at higher oxidation temperatures i.e above 75°C, the particles either transform into α-Fe_2O_3 or break into smaller α-FeOOH particles. At intermediate temperatures the length of the particles do not increase and only few of the particles break into smaller particles. However, the width of the particle increase with an increase in the oxidation temperature from 20 to 75°C.

IV.4.5. DISCUSSION

Precipitation and oxidation of aqueous Fe^{2+} may result in the production of a number of iron oxyhydroxides and oxides depending upon the method of preparation, iron precursor, and other experimental conditions. The data show that the [Fe]/[OH^-] ratio, the oxidizing agent and the reaction rate play key roles in determining the crystalline structure of iron oxyhydroxides or oxides. On the other hand, the oxidation temperature mainly control the particle size rather than morphology. At higher oxidation temperatures (i.e > 75°C) the morphology as well as the particle sizes are affected.

Kiyama et al (IV.4.17,IV.4.18) studied the oxidation of Fe(II) in acid chloride solutions in the pH range of 2 to 5 and in the temperature range of 15 to 80°C. The authors used a mixture of gaseous ammonia and air in order to control the pH. Their results showed the formation of α-, β-, γ-FeOOH and α-Fe_2O_3, or an amorphous precipitate, depending on the pH and oxidation temperature. The pH value decreased with an increase of the oxidation time, and at the end of the oxidation, the pH value was found to be increased rapidly to 7 or greater. The surface areas of the resulting iron oxyhydroxides or oxides ranged from 54 to 127 m^2/g. The BET areas are comparable with the results from the present work. Contrary to the data of Kiyama et al., the present data show a gradual decrease in the pH value during the oxidation of Fe^{2+}.

The crystalline phases and morphologies of iron compounds depend significantly on the reaction conditions such as temperature, pH, coexisting ions etc. For example spherical (IV.4.19), cubic (IV.4.20,IV.4.21), spindle-type (IV.4.22), doubly

spherical (IV.4.23), and disc like (IV.4.24) α-Fe_2O_3 were prepared by the hydrothermal treatment of iron salt solutions at elevated temperature. Kameshwari reported (IV.4.25) the formation of δ-FeOOH, α- and γ-Fe_2O_3 (needle shape) starting from $FeSO_4$, β-FeOOH (spherical shape) from $FeCl_3$, and α-FeOOH (irregular shape) particles starting from $Fe(NO_3)_3$ precursors. The variation of the morphology of iron oxyhydroxides or oxides has been attributed due to the effect of anions.

TEM results of α-FeOOH from the present study also show the formation of well defined needle shaped α-FeOOH particles starting from $FeSO_4$ salt solutions (see Figure IV.4.9). However, Atkinson et al (IV.4.26) reported the synthesis of well defined needle shape α-FeOOH particles starting from ferric nitrate solutions. Atkinson et al also showed that the particle growth is preferential in the [001] direction compared to [100] or [010] directions. These authors also reported that the crystal sizes commonly range from 0.01 to 0.03 μ (10 to 30 nm) in width and from 0.1 to 0.4 μ (100 to 400 nm) in length. The results from the present study show a particle size ranging from 50 to 5000 nm depending on the oxidation temperature for α-FeOOH samples, 30 to 110 nm for magnetite sample, and 30 to 150 nm for δ-FeOOH sample. An estimation of L/W values for α-FeOOH particles from Atkinson's work shows that the values are in the range of 10 and the results from the present study show particle L/W values that vary from 3 to 27 in the oxidation temperature range of 7 to 75°C. The disagreement between these two results can be attributed to the different starting materials for making α-FeOOH as well as different preparation methods. The BET areas for the α-FeOOH samples prepared from ferrous sulfate range from 25 to 89 m^2/g which is approximately in the same range of those reported (14 to 78 m^2/g) by

Atkinson et al (IV.4.26). Van Der Woude and De Bruyn (IV.4.27,IV.4.28) reported the synthesis of monodispersed goethite (α-FeOOH) particles by controlled dialysis of dispersions of amorphous iron hydroxide primary particles. In another method, seeds of goethite crystals were added to supersaturated iron-containing solutions (ferric nitrate solutions). Their experiments confirmed that the goethite crystals grow in the [001] direction by incorporation of low-molecular weight species from solution. Their electron microscopy studies of these samples showed after dialysis of 1 M Fe(NO3)3 solution the development of particles with very large length dimension. According to Van Der Woude and De Bruyn (IV.4.27,IV.4.28) the particle sizes are in the range of 4 to 150 nm in length while the width was between 4 to 20 nm and the approximate L/W values range from 1 to 10 nm. Comparing the particle sizes reported by Van Der Woude and De Bryun (IV.4.27,IV.4.28) with the results from the present study indicate that the particle sizes (length, width, and L/W) are very much dependent on the method of preparation, and sarting iron precursor.

IV.4.6. CONCLUSIONS

α-FeOOH with controlled crystallinity, size and morphology can be synthesized in slightly alkaline media by the oxidation of aqueous iron (II) ions by controlling the $[Fe^{2+}]/[OH^-]$ ratio, oxidizing agent and oxidation temperature. The initial $Fe^{2+}:OH^-$ mole ratio strongly influences the nature of the final product during the oxidation of ferrous hydroxide aqueous suspensions. The morphology of the oxyhydroxide products vary systematically with an increase in oxidation temperature. At low oxidation temperatures (7°C) the iron oxyhydroxide does not show a particular morphology. On the other hand, as the oxidation temperature increases to 20°C a

well defined acicular α-FeOOH particle formation was observed. At higher oxidation temperatures (~75°C) the formation of acicular α-FeOOH as well as α-Fe_2O_3 (spherical) particles were observed.

IV.4.7. REFERENCES

IV.4.1. A. A. Olowe and J. M. R. Genin, *Corrosion Science*, **32**, 965 (1991).

IV.4.2. J. D. Bernal, D. R. Dasgupta, and A. L Mackay, *Clay Miner. Bull*, **4**, 15 (1959).

IV.4.3. T. Misawa, K. Hashimoto, W. Suetaka, and S. Shimodaira, *J. Inorg. Nucl. Chem*, **35**, 4159 (1973).

IV.4.4. T. Misawa, K. Hashimoto and S. Shimodaira, *J. Inorg. Nucl. Chem.*, **35**, 4167 (1973).

IV.4.5. Y. Tamaura, T. Yoshida and T. Katsura, *Bull. Chem. Soc. Japan*, **57**, 2411 (1984).

IV.4.6. A. A. Olowe, PH. Refait and J. M. R. Genin, *Corrosion Science*, **32**, 1003 (1991).

IV.4.7. H. C. B. Hansen, *Clay Minerals*, **24**, 663 (1989).

IV.4.8. W. Feitknecht, *Helv. Chim. Acta*, **24**, 676 (1941).

IV.4.9. R. Allman, *Chimica*, **24**, 99 (1970) .

IV.4.10. T. Misawa, K. Hashmoto and S. Shimodaira, *Corrosion Science*, **14**, 131 (1974).

IV.4.11. N. S. Clarke, and P. G. Hall, *Langmuir*, **7**, 672 (1991).

IV.4.12. S. Brunuaer, P. H. Emmett and E. Teller, *J. Amer. Chem. Soc.*, **60**, 309 (1938).

IV.4.13. J. C. P. Broekhoff and J. H. deBoer, *J. Catal.*, **9**, 15 (1967).

IV.4.14. R. Lin, R. Srinivasn and B. H. Davis., submitted.

IV.4.15. K. S. W. Sing, D. H. Everett, R. A. W. Haul, L. Moscou, R. A. Pierotti, J. Rouquerol and T. Siemieniewska, *Pure & Appl. Chem.*, **57**, 603 (1985).

IV.4.16. P. H. Klug and L. E. Alexander, in X-ray Diffraction Procedures, John Wiley & Sons Inc., NY 1954, p491.

IV.4.17. M. Kiyama and T. Takada, *Bull. Chem. Soc. Japan*, **47**, 1646 (1974).

IV.4.18. M. Kiyama, T. Akita and T. Takada, *Bull. Inst. Chem. Res, Kyoto Univ.*, **61**, 335 (1983).

IV.4.19. E. Matijevic and P. Scheiner, *J. Colloid Interface Sci.*, **63**, 509 (1978).

IV.4.20. S. Hamada and E. Matijevic, *J. Colloid Interface Sci.*, **84**, 274 (1981).

IV.4.21. M. Ozaki, S. Krathohvil and E. Matijevic, *J. Chem. Soc. Faraday Trans I*, **78**, 2147 (1982).

IV.4.22. S. Hamada and E. Matijevic, *J. Colloid Interface Sci.*, **102**, 146 (1986).

IV.4.23. S. Hamada, S. Niizeki and Y. Kudo, *Bull. Chem. Soc. Japan*, **59**, 3443 (1986).

IV.4.24. R. S. Sapieszko and E. Matijevic, *J. Colloid Interface Sci.*, **74**, 405 (1980).

IV.4.25. S. Kameshwari, Symposium on Science of Catalysis and its Application to Industry., held at FPDIL, Sindri, India, 1979.

IV.4.26. R. J. Atkinson, A. M. Posner and J. P. Quirk, *J. Inorg. Nucl. Chem.*, **30**, 2371 (1968).

IV.4.27. J. H. A. Van Der Woude and P. L. De Bruyn, *Colloids and Surfaces*, **9**, 173 (1984).

IV.4.28. J. H. A. Van Der Woude and P. L. De Bruyn, *Colloids and Surfaces*, **12**, 179 (1984).

Table IV.4.1

Effect of Oxidizing Agent, [Fe]/[OH^-] Ratio on the Crystal Structure and Surface Area of Iron Oxyhydroxides or Oxides

S. No.	[Fe]/[OH]	Oxidizing Agent	XRD Results	BET Surface Area, m^2/g
1	0.2	O_2	α-FeOOH	25.1
2	0.2	H_2O_2	δ-FeOOH with trace α-FeOOH	46.8
3	0.5	O_2	Fe_3O_4	60.3
4	3.0	O_2	α-FeOOH	46.4
5	3.0	H_2O_2	β-FeOOH trace α-FeOOH	15.2

Table IV.4.2

Oxidation of Ferrous Hydroxide Aqueous Suspension with Molecular Oxygen at Different Temperatures (Precipitating Agent is NaOH, O_2 Flow is 45cc/min., and Total Volume of the Reaction Mixture is 1500 cc)

S.No.	Sample Code	Iron Concentration, M	[Fe]/[OH]	Oxidation Temperature, °C	Final pH	BET Surface Area, m^2/g (Dried)	XRD Results	Crystallite Sizes, A
1	Raj42	0.2	3.008	7	4.13	89.3 (0.28)#	α-FeOOH	1. 51 (110) 2. 59 (120) 3. 4. 63 (111) 5. 53 (221) 6. 108 (131)
2	Raj43	0.2	2.965	20	3.68	82.8 (0.36)#	α-FeOOH	1. 112 (110) 2. 127 (120) 3. 171 (130) 4. 112 (111) 5. 111 (221) 6. 143 (151)
3	Raj41-E	0.2	3.008	40	3.04	69 (0.57)#	α-FeOOH	1. 137 (110) 2. 159 (120) 3. 219 (130) 4. 210 (111) 5. 148 (221) 6. 168 (151)
4	Raj39-E	0.2	3.001	55	2.64	50.9 (0.61)#	α-FeOOH	1. 190 (110) 2. 163 (120) 3. 227 (130) 4. 204 (111) 5. 167 (221) 6. 265 (151)
5	Raj40-B	0.2	2.964	75	2.68	39.8 (0.48)#	α-FeOOH, α-Fe_2O_3 & γ-Fe_2O_3 (Traces)	1. 186 9110) 2. 169 (120) 3. 249 (130) 4. 210 (111) 5. 156 (221) 6. 226 (151)

Pore volume cc/gram.

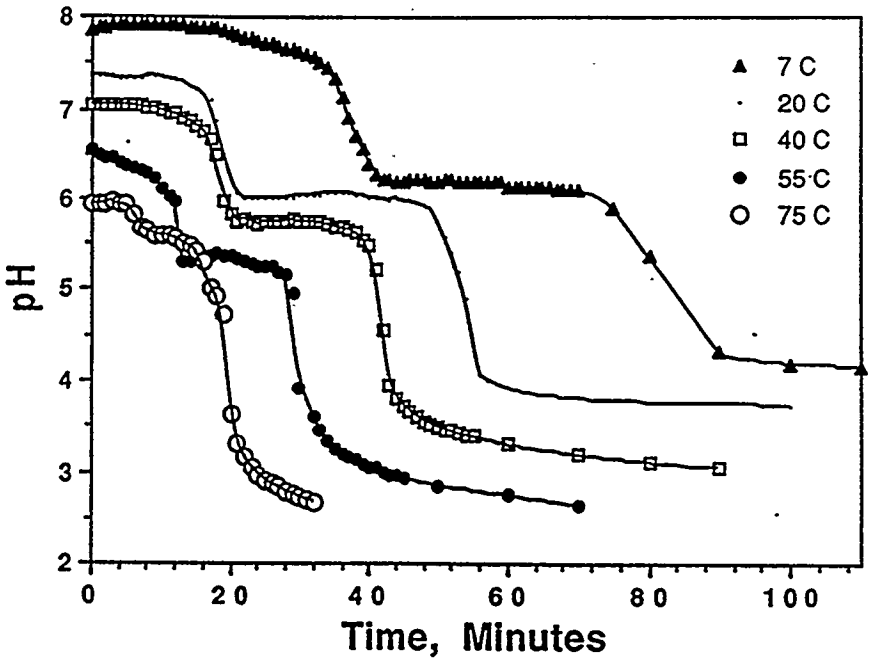

Figure IV.4.1. pH vs oxidation time during the oxidation of Fe(II) in aqueous solution with molecular oxygen. (a) -▲- = 7°C, (b) - · - = 20°C, (c) -□- = 40°C, (d) -●- = 55°C and (e) -○- = 75°C.

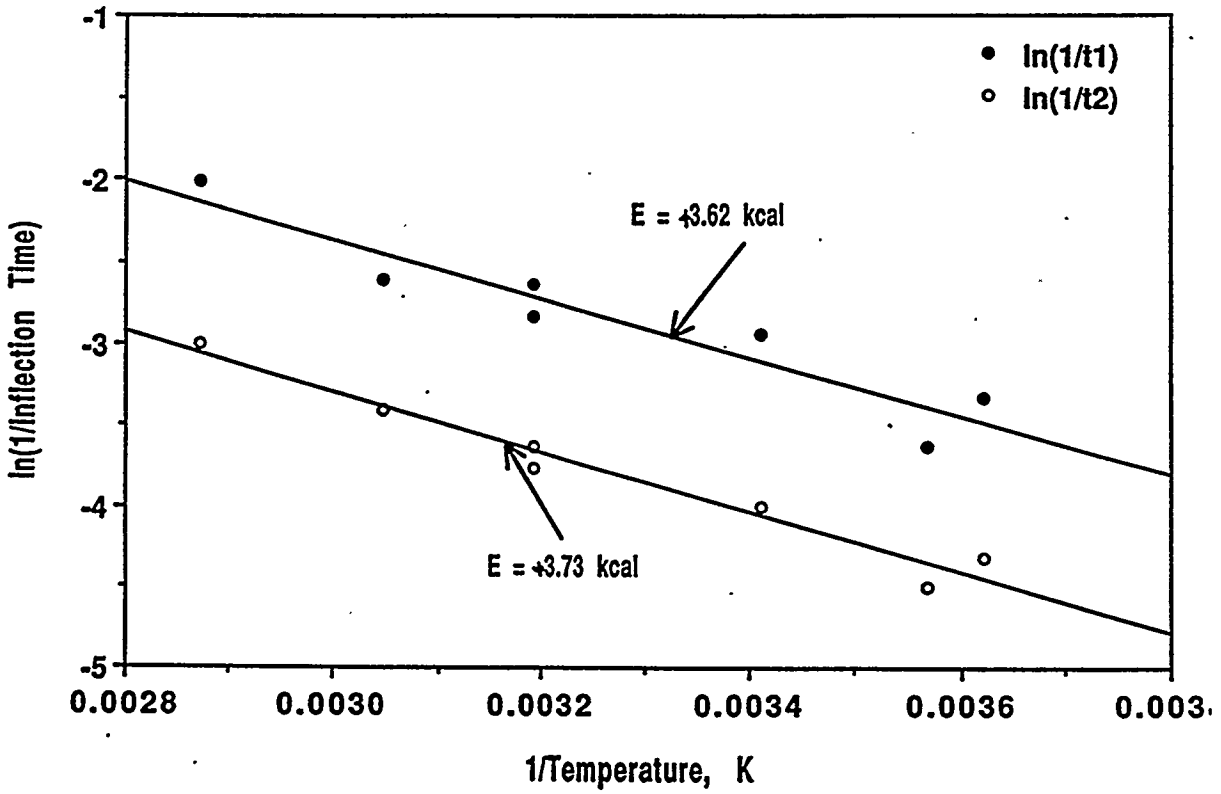

Figure IV.4.2. ln (inflection) times vs 1/T. (a) -●- t_1 and (b) -○- t_2.

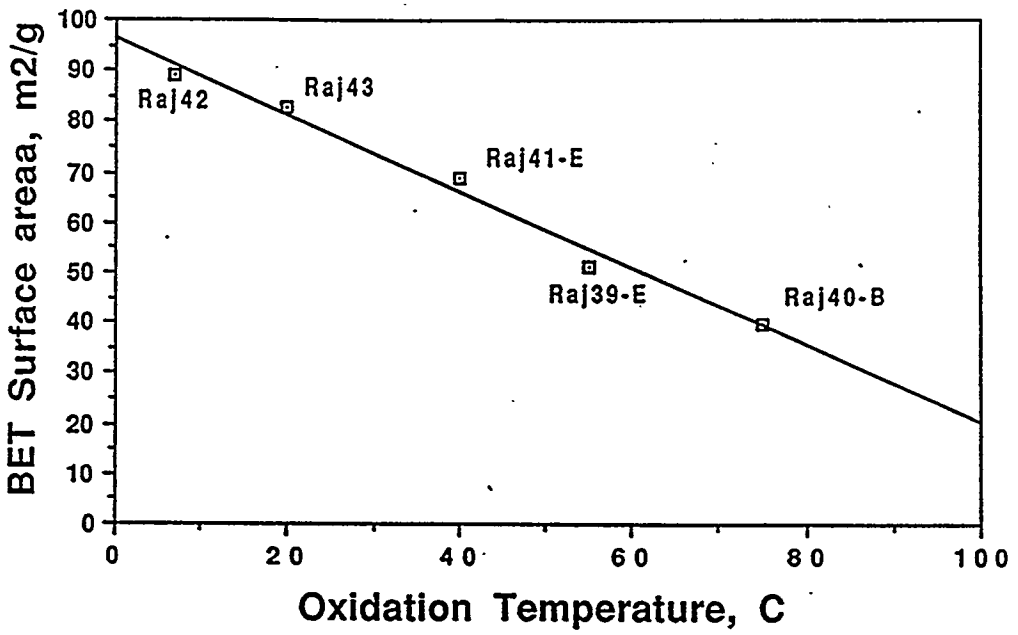

Figure IV.4.3. Effect of oxidation temperature on the BET surface area of α-FeOOH samples.

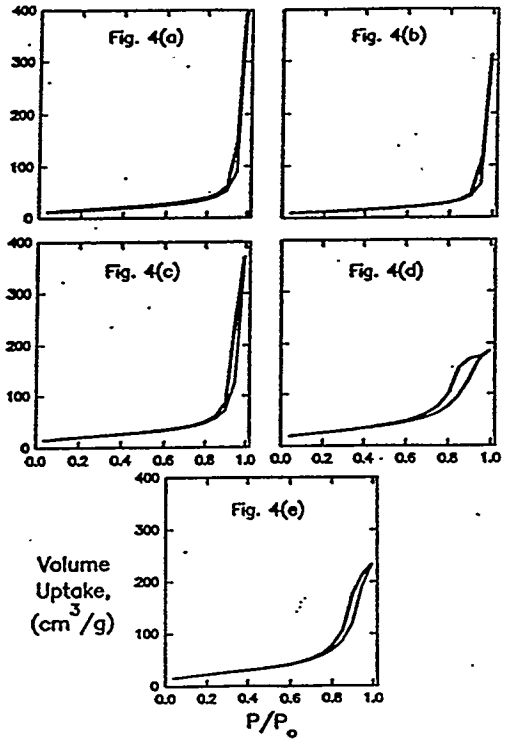

Figure IV.4.4. Nitrogen adsorption and desorption isotherms for the α-FeOOH samples prepared at different oxidation temperatures. (a) 7°C, (b) 20°C, (c) 40°C, (d) 55°C, and (e) 75°C. - + - Adsorption and -●- Desorption.

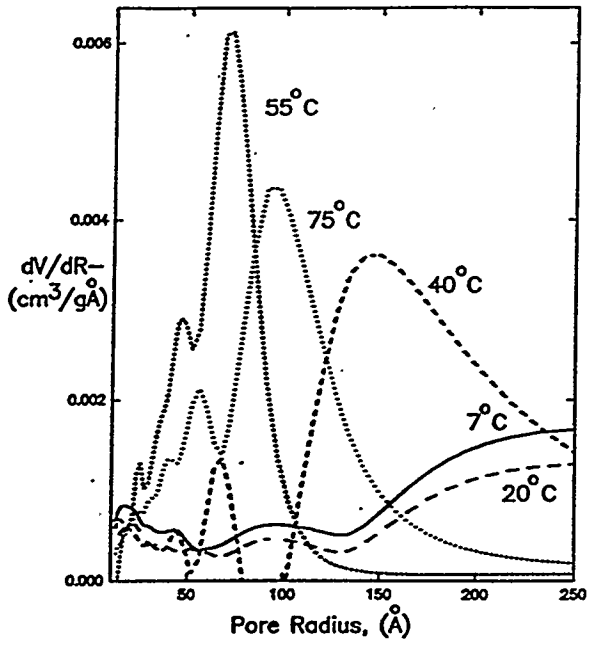

Figure IV.4.5. Effect of oxidation temperature on the pore size distributions for α-FeOOH samples prepared at different temperatures. (a) 7°C, (b) 20°C, (c) 40°C, (d) 55°C, and (e) 75°C.

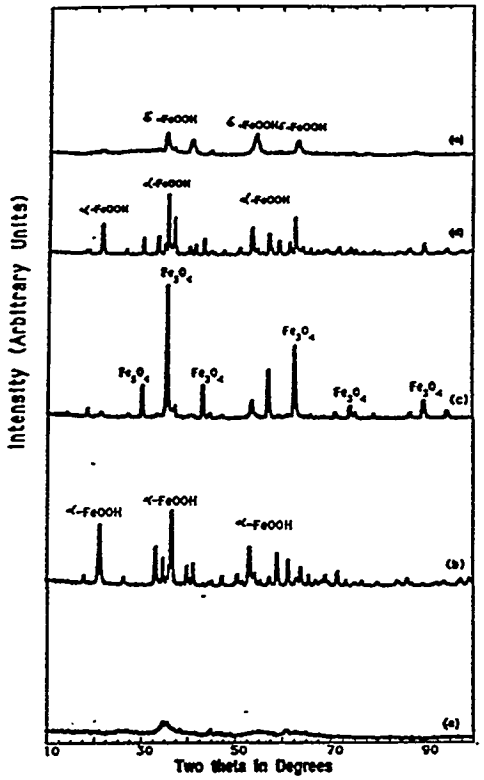

Figure IV.4.6. Effect of oxidizing agent and [Fe]/[OH-] ratio on the crystal structure of iron oxides or oxyhydroxides. (a) [Fe]/[OH^-] = 3.0 and oxidizing agent is aq. H_2O_2, (b) [Fe]/[OH^-] = 3.0 and oxidizing agent is oxygen, (c) [Fe]/[OH^-] = 0.5 and oxidizing agent is oxygen, (d) [Fe]/[OH^-] = 0.2 and oxidizing agent is oxygen, (e) [Fe]/[OH^-] = 0.2 and oxidizing agent is aq. H_2O_2.

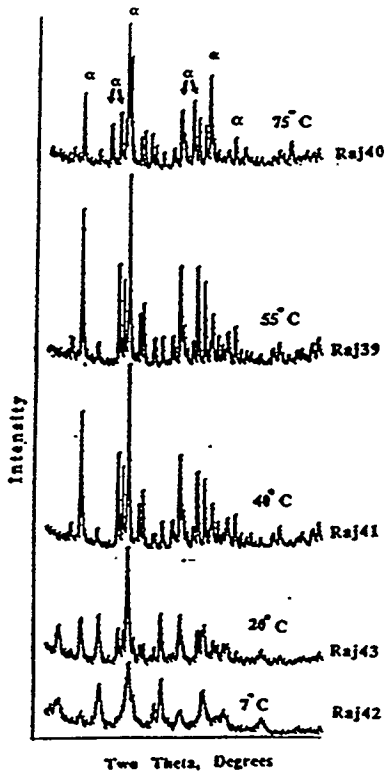

Figure IV.4.7. Oxidation of ferrous hydroxide aqueous suspension with molecular oxygen at different temperatures. (a) 7°C, (b) 20°C, (c) 40°C, (d) 55°C, and (e) 75°C.

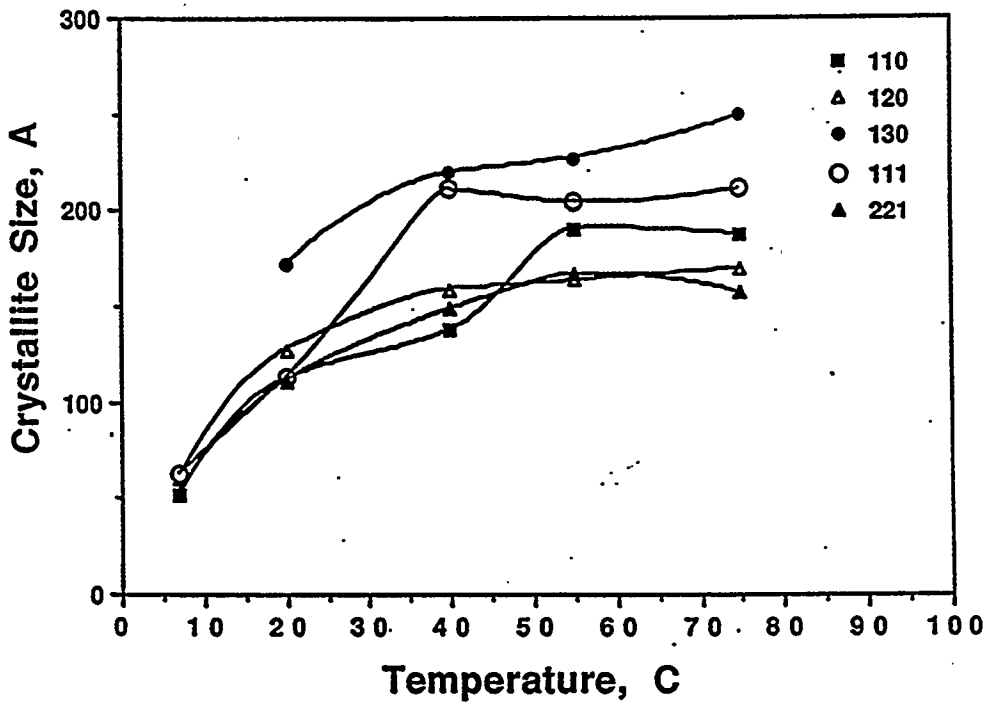

Figure IV.4.8. Crystallite size vs oxidation temperature at different crystalline planes. -■- 110 plane, -△- 120 plane, -●- 130 Plane, -○- 111 Plane, -▲- 221 plane.

Figure IV.4.9. Transmission Electron Micrograph(TEM) of α-FeOOH Prepared at 55°C at [Fe]/[OH] ratio = 3.0.

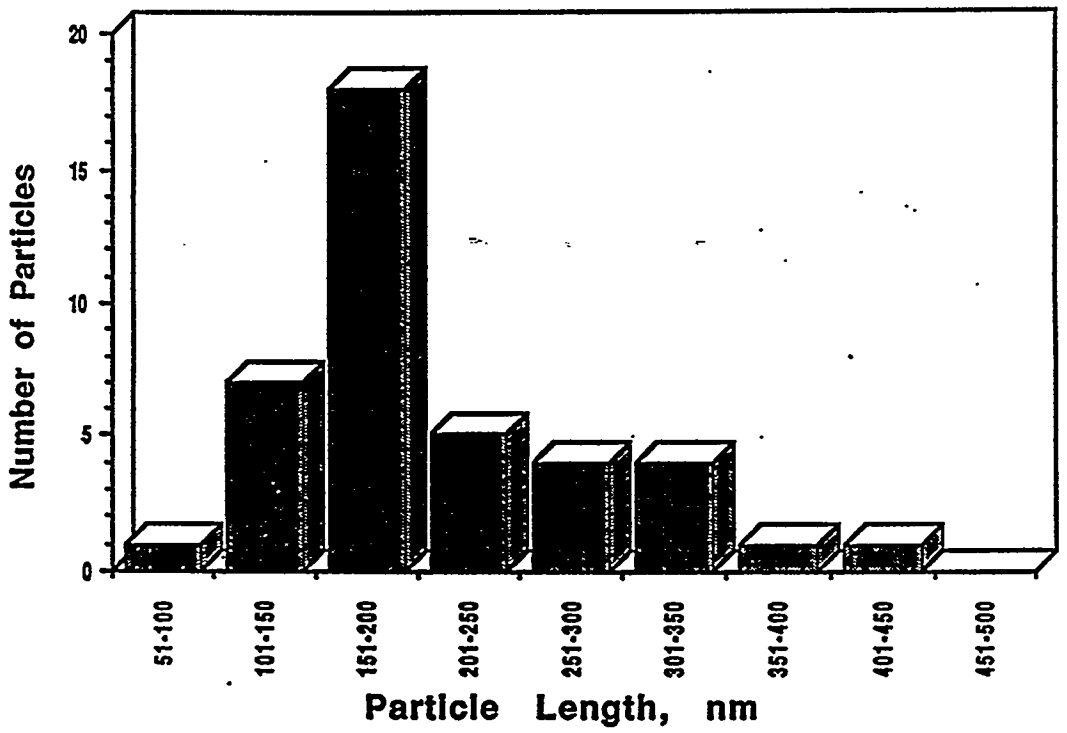

Figure IV.4.10. Particle size (length) distribution for α-FeOOH sample prepared at 55°C.

Figure IV.4.11. Transmission electron micrograph (TEM) of Fe_3O_4.

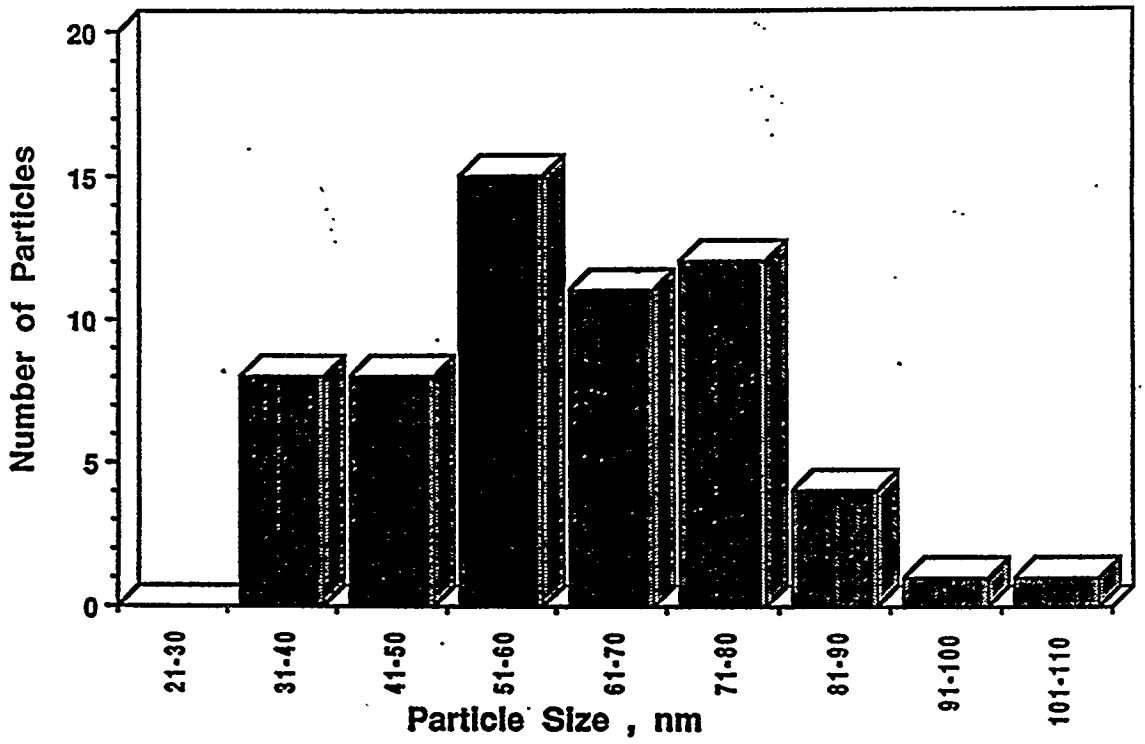

Figure IV.4.12. Particle size distribution for the the Fe_3O_4 sample.

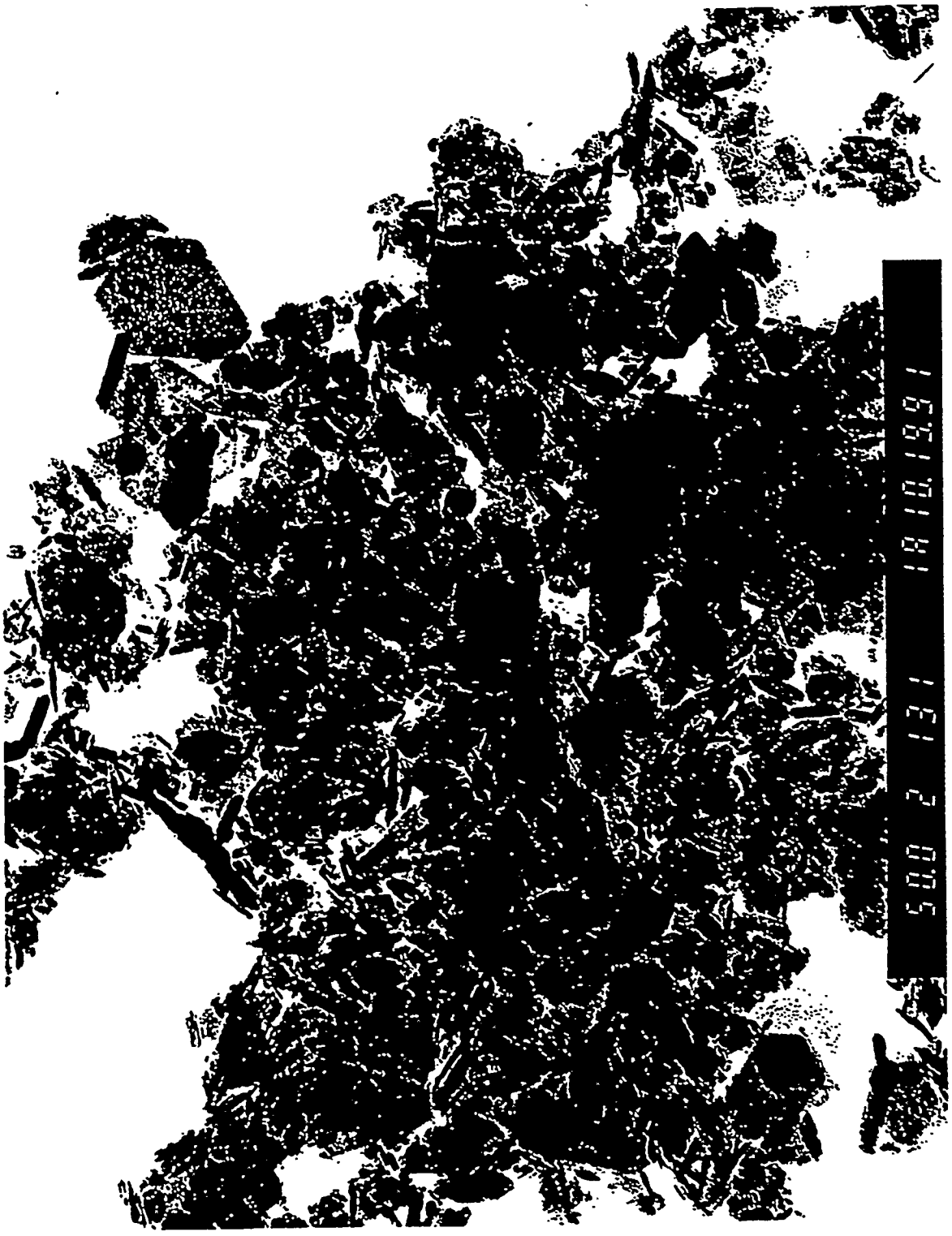

Figure IV.4.13. Transmission electron micrograph (TEM) of δ-FeOOH.

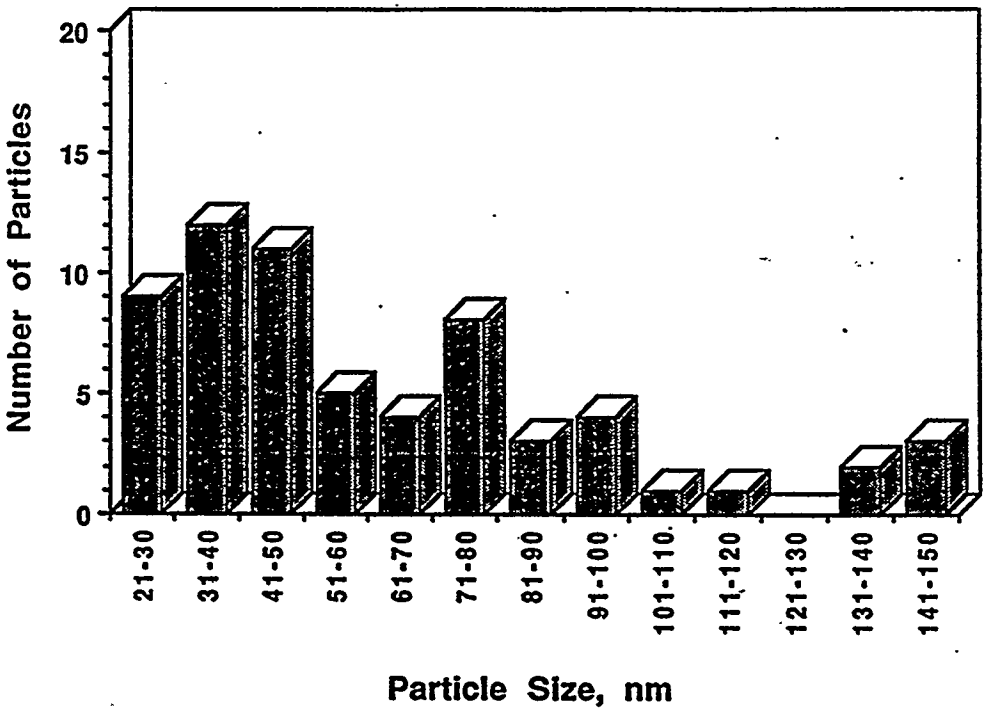

Figure IV.4.14. Particle size distribution for δ-FeOOH.

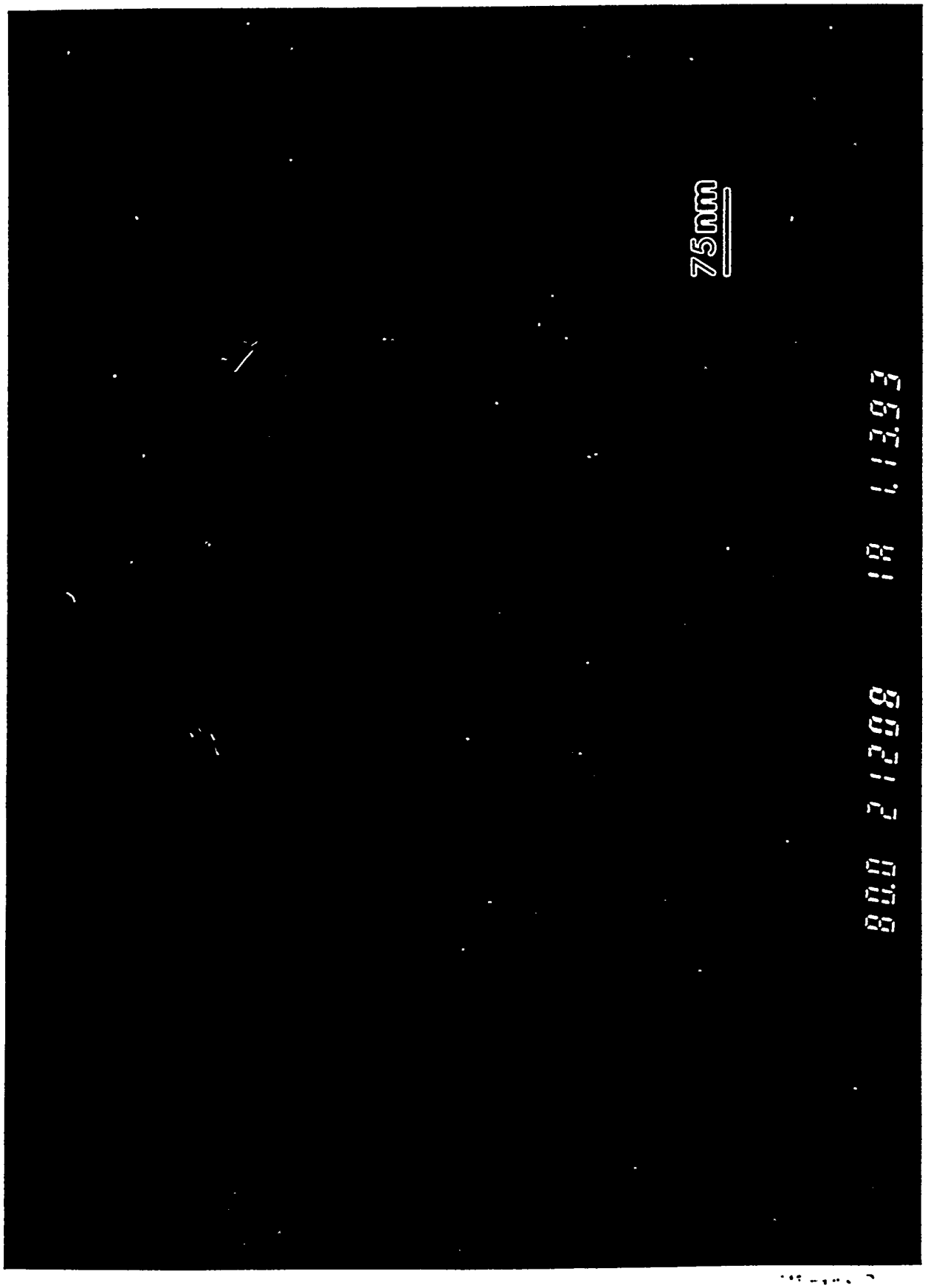

Figure IV.4.15. Transmission electron micrograph for the α-FeOOH sample prepared at 7°C.

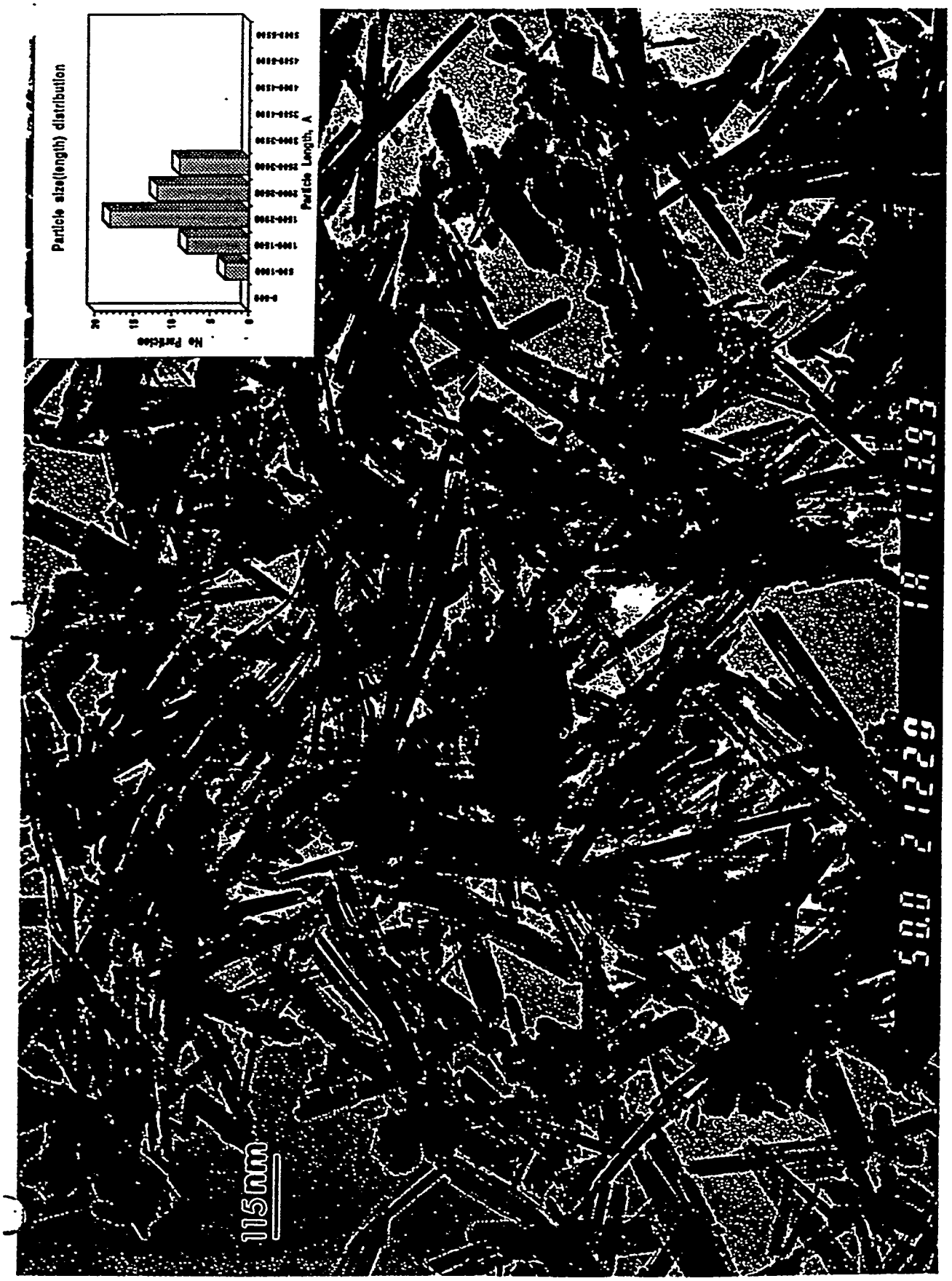

Figure IV.4.16. Transmission Electron Micrograph of α-FeOOH prepared at 40°C. (inset represents the particles size distribution).

Figure IV.4.17. Transmission Electron Micrograph of α-FeOOH prepared at 75°C.

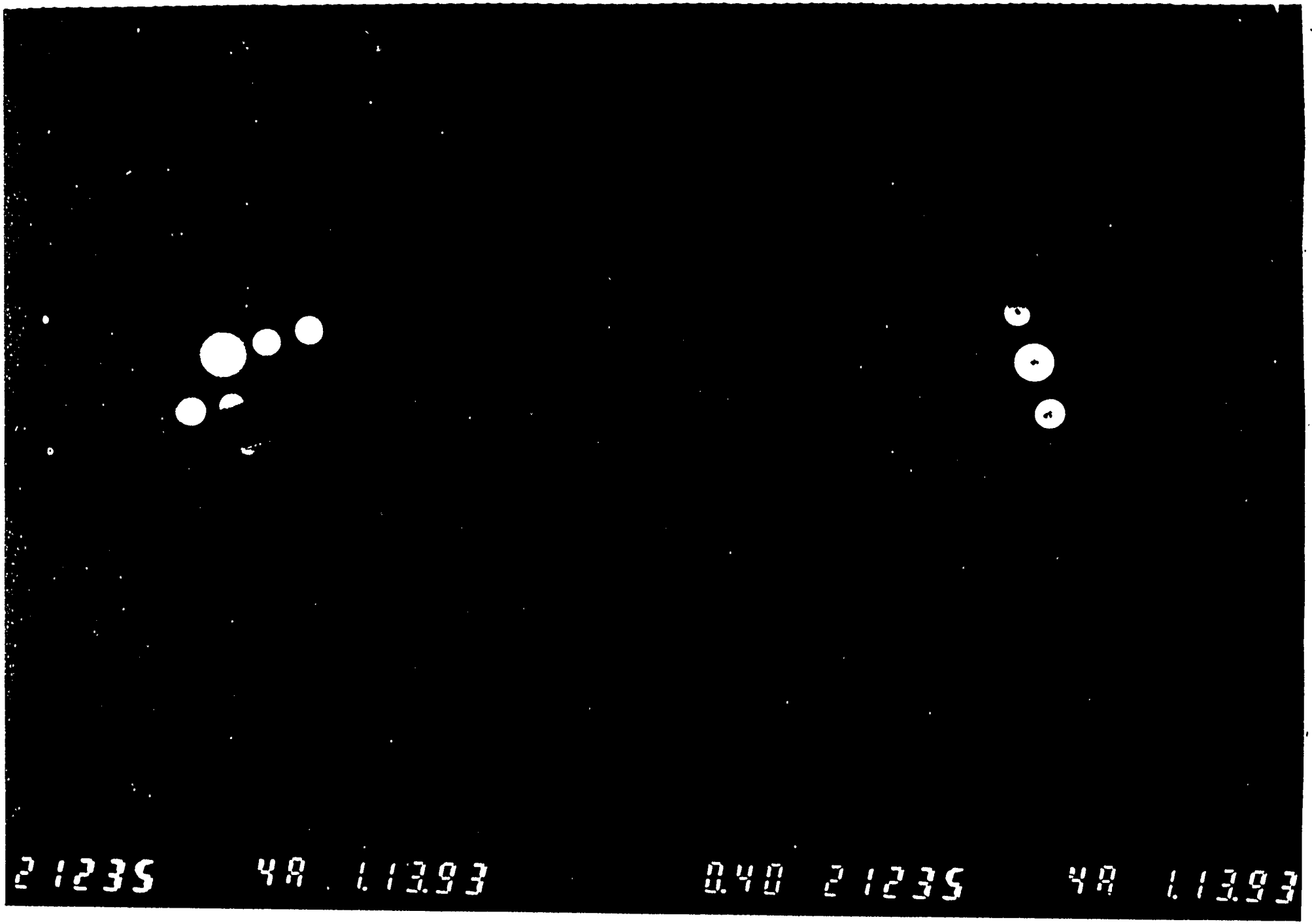

Figure IV.4.18. Electron Microdiffraction patterns of (a) α-FeOOH (needle shape) and (b) α-

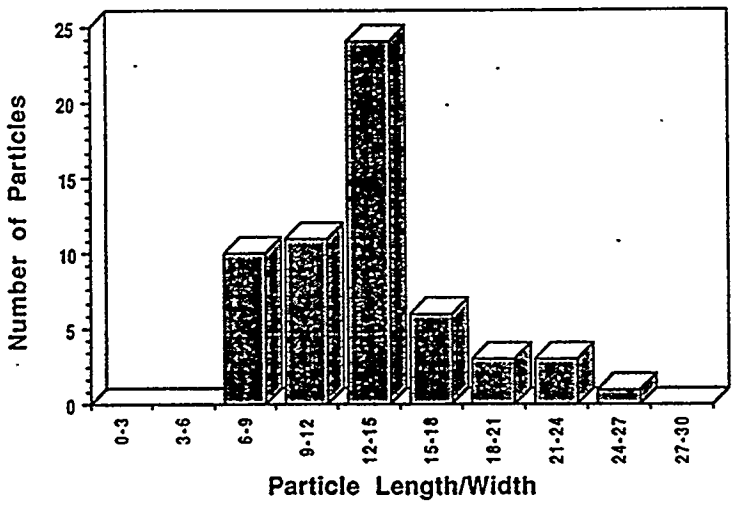

Figure IV.4.19. Length/width ratio distribution for α-FeOOH particles prepared at 20°C.

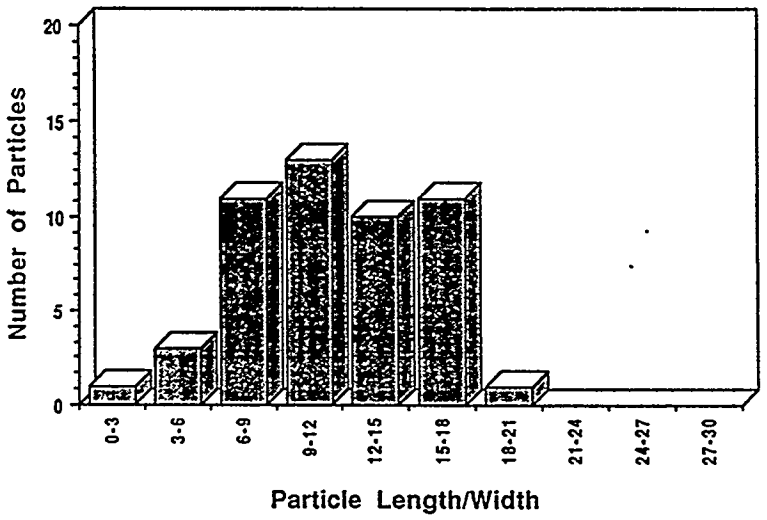

Figure IV.4.20. Length/width ratio distribution for α-FeOOH particles prepared at 40°C.

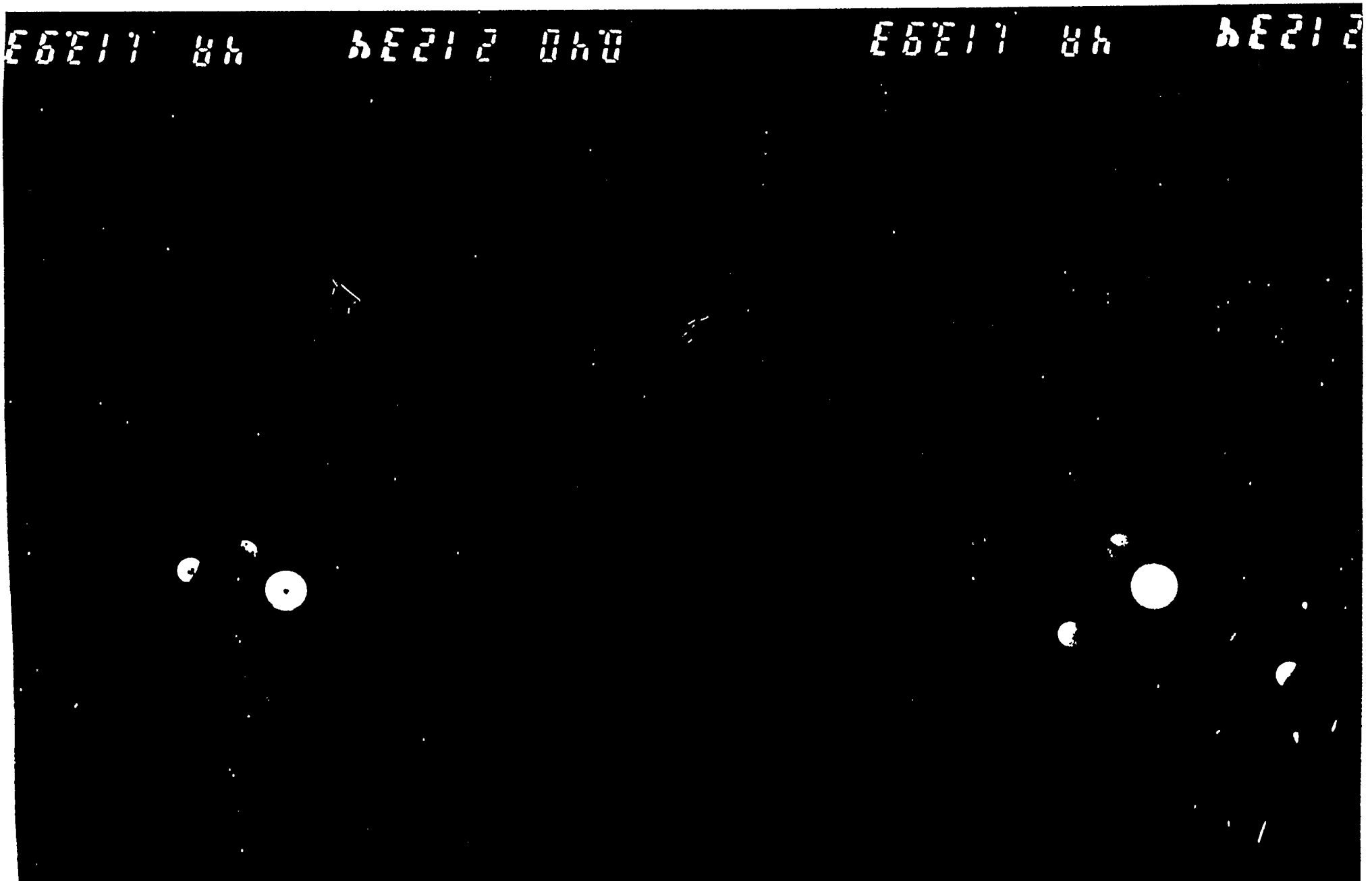
E6E11 UA AE212 0A0
E6E11 UA AE212

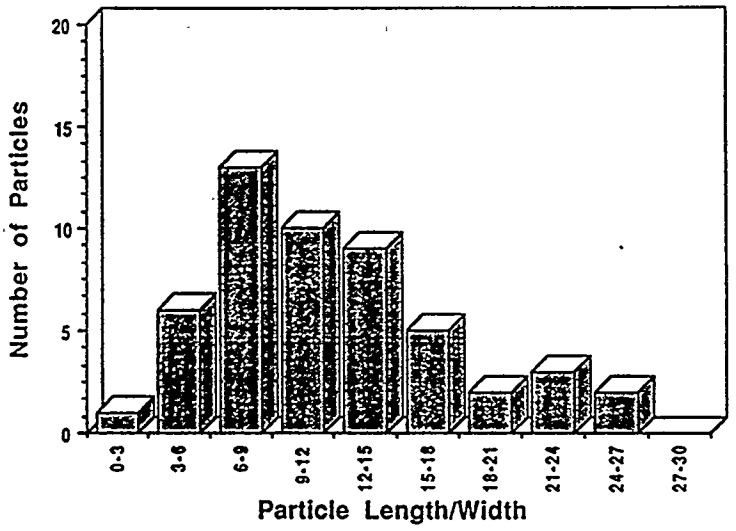

Figure IV.4.21. Length/width ratio distribution for α-FeOOH particles prepared at 55°C.

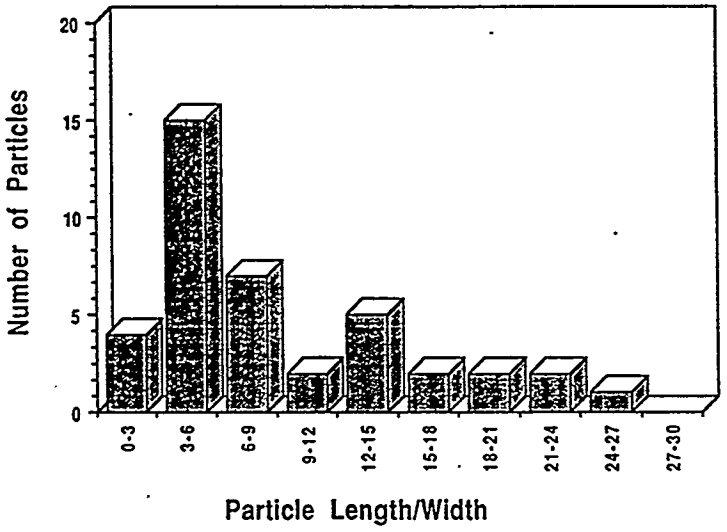

Figure IV.4.22. Length/width ratio distribution for α-FeOOH particles prepared at 75°C.